Journal of Engineering Mathematics **39:** 47–62, 2001.

Separating shear flow past a surface-mounted blunt obstacle

S. BHATTACHARYYA[1], S.C.R. DENNIS[2] and F.T. SMITH[3]
[1]*Department of Mathematics, Indian Institute of Technology, Kharagpur, 721302, West Bengal, India*
[2]*Dept. of Applied Mathematics, University of Western Ontario, London, Ontario, Canada, N6A 5B7*
[3]*Department of Mathematics, University College London, Gower Street, London WC1E 6BT, UK*

Received 28 October 1999; accepted in revised form 25 May 2000

Abstract. The planar flow of incompressible fluid past a blunt obstacle mounted on a flat (horizontal) fixed solid surface of infinite extent is examined in the presence of an incident linear velocity profile, modelling the fluid behaviour close to a small surface roughness for instance. The motion is taken to be steady and laminar. The obstacle is blunt in the sense that its typical surface slopes are not small, a feature which here always induces flow separation both upstream and downstream of the obstacle. Computations and nonlinear theory are applied, together with comparisons. The direct computations of the Navier-Stokes equations, using for example a higher order upwind-difference scheme, deal with a moderate range of Reynolds numbers up to 200, based on the obstacle height and the incident uniform shear. In addition the accuracy is necessarily limited as the Reynolds number increases. The theory is for large Reynolds numbers and is based on viscous-inviscid reasoning, back-pressure effects from the obstacle and slender-layer separation locally, among other influences. The comparisons nevertheless yield encouragingly close agreement, for the present computed cases of a vertical flap or a rectangular block. This is both quantitatively, in terms of the upstream separation and downstream reattachment positions in particular, and generally, in terms of the separating flow structure, even at the notably moderate Reynolds numbers covered accurately by the computations.

Key words: blunt roughness, computations, separation, theory

1. Introduction

Configurations involving shear flow over a blunt obstacle, mounted on an otherwise flat or nearly flat surface, are manyfold and have much physical and technological interest. A blunt or bluff obstacle here is one whose typical surface slopes are of order unity or greater, such as a flap standing normal to the flat surface, a rectangular block, a forward-facing step or a hemispherical object. Configurations of practical interest include boundary-layer flow past roughnesses on airfoils and turbine blades, atmospheric boundary layer motion over hills, wind over water, the use of trip wires to generate transition to turbulent flow downstream, the flow past excrescences in pipes or at artery walls, and the Gurney-flap device placed near an airfoil or blade trailing edge. Some of the theoretical and/or computational studies relevant to the above configurations and especially to the present research are by Dennis and Smith [1], Mei and Plotkin [2], Durst and Loy [3] on internal flows, Savin *et al.* [4] on transition, Smith and Walton [5] on roughness flows, and Giguère *et al.* [6], Smith [7] on the advantages of a flap device being buried within the trailing-edge boundary layer; but see also the many references therein on computations, theory and experiments.

Our specific concern is with the case of a blunt obstacle so small and close to the flat surface that the surrounding fluid motion, *i.e.* the farfield flow as far as the scale of the obstacle is concerned, may be viewed as uniform shear flow. The whole motion is taken to be laminar,

planar and steady, and the fluid to be incompressible and Newtonian, yielding an idealised setting of course but one which has correspondingly clearer findings, it is hoped, and which is fundamental to all the practical configurations of interest. Computation and theory are applied for the determination of the major flow properties and for their basic understanding. The theory, which is for large Reynolds numbers, is meant to provide extra insight of course but it also gives particular predictions, for example for the positions of separation upstream and reattachment downstream of the obstacle, and it helps to guide the all-important numerical gridding, especially at increasing Reynolds numbers. The quite large-scale computation is needed at almost all moderate Reynolds numbers and it helps to indicate the range of practical validity of the theory, how much the flow solution is independent of the precise shape of obstacle, and so on. The joint approach using computation and theory is very much a hand-in-hand one. A not dissimilar approach has also been used successfully on occasion in studies of external flow past a blunt body, without surface mounting, as in many papers on the subject by Dennis, Sychev, Fornberg, Smith, Chernyshenko and co-workers: *e.g.* see review in [8, Chapters 23–25].

Section 2 below describes the flow set-up, for the surface-mounted obstacle in a uniform-shear flow, at finite Reynolds number based on the typical obstacle height and on the slope of the incident velocity profile at the flat surface. Computational methodology is presented in detail in Section 3; compare the local leading-edge and trailing-edge studies by Van de Vooren, Dijkstra, Veldman in the 1970s (*e.g.* see [8, Chapters 23–25]). The present computations are designed especially for obstacles which are vertical flaps or rectangular blocks, although the accuracy is of course limited. Theory for large Reynolds numbers is given in Section 4, this being quite distinct from the small-disturbance linear analyses of Stewartson [9], Smith [10] because in the current setting the physical slopes present are not small and so they demand nonlinear reasoning. While intuition may at first suggest that, with increasing Reynolds number, the recirculating eddy upstream of the obstacle should shrink due to inertial effects, the subsequent action of viscous effects near the upstream surface implies that the eddy must elongate, for overall smoothness of the separating flow. This is reflected in the prediction of the separation position (far) upstream, and likewise in the predicted reattachment station (far) downstream. Moreover, the arguments used generalize, for example to any obstacle shape, and they simplify certain related ones used previously, enabling the upstream separation point for instance to be obtained from a single, rapid, forward numerical march. Section 5 shows results and comparisons between computation and theory. Section 6 provides further comments.

2. The flow configuration

The blunt shaped obstacle of concern is on a fixed surface, is deep inside the surface boundary layer or other shear flow and is so localized that the surface appears flat and indefinitely long (the x axis) and the fluid appears to be of semi-infinite extent normally, with uniform incident shear flow. This implies that the only relevant geometric length scales are those of the obstacle itself. We take the typical height of the obstacle as the flow's characteristic length scale ℓ^*, which is often comparable with the typical obstacle length anyway for a blunt shape. Further, as there is no velocity scale u^* directly we take the prescribed slope λ^* of the incident velocity profile at the surface multiplied by ℓ^*, leaving $u^* = \lambda^*\ell^*$ as the velocity scale based on the obstacle height. Nondimensional quantities are then used, so that in Cartesian coordi-

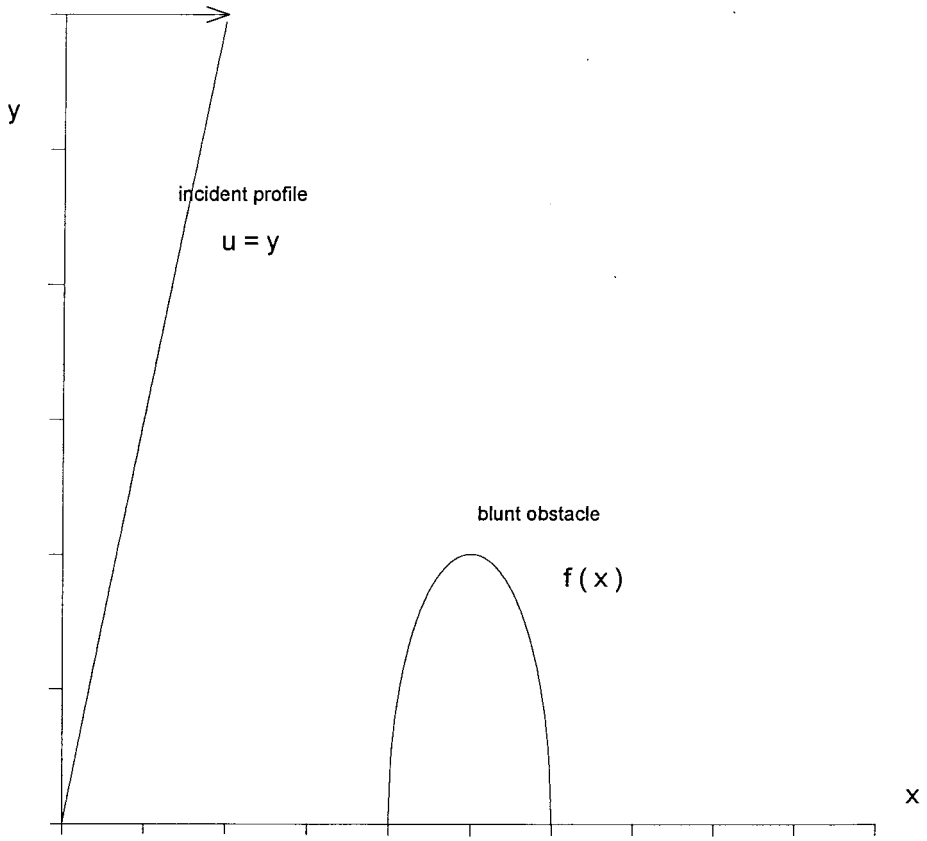

Figure 1. Sketch of the flow configuration, in nondimensional terms, for a blunt obstacle (smooth or non-smooth) with $|f'|$ typically of order unity.

nates $\ell^*(x, y)$ which are streamwise and normal respectively the corresponding fluid velocity $\lambda^*\ell^*(u, v)$ and pressure $\rho^*\lambda^{*2}\ell^{*2}p$ satisfy the continuity and Navier-Stokes equations

$$\frac{\partial u}{\partial x} + \frac{\partial v}{\partial y} = 0, \qquad u\frac{\partial u}{\partial x} + v\frac{\partial u}{\partial y} = -\frac{\partial p}{\partial x} + \mathrm{Re}^{-1}\nabla^2 u, \tag{2.1a,b}$$

$$u\frac{\partial v}{\partial x} + v\frac{\partial v}{\partial y} = -\frac{\partial p}{\partial y} + \mathrm{Re}^{-1}\nabla^2 v. \tag{2.1c}$$

Here the shear-based Reynolds number $\mathrm{Re} \equiv \lambda^*\ell^{*2}/\nu^*$ has characteristic values of order unity, the constants ρ^*, ν^* denote in turn the density and kinematic viscosity of the incompressible fluid, and ∇^2 is the Laplacian $\partial^2/\partial x^2 + \partial^2/\partial y^2$. The governing Equations (2.1a–c) hold above the obstacle in the upper half plane. They are subject to the boundary conditions

$$u = v = 0 \text{ at } y = f(x), \qquad u \sim y,\ v \to 0 \text{ as } x^2 + y^2 \to \infty, \tag{2.1d,e}$$

for no slip at the given nondimensional surface $f(x)$ of the obstacle or flat plate and for the approach to the specified uniform shear flow in the farfield, respectively. See Figure 1.

The task is to solve (2.1a-e), then. An alternative to (2.1a) is to use a stream function ψ defined by $u = \partial\psi/\partial y,\ v = -\partial\psi/\partial x$ with, say, ψ zero on the obstacle surface, and of course (2.1b,c) can be combined into the vorticity equation

$$u\frac{\partial\zeta}{\partial x} + v\frac{\partial\zeta}{\partial y} = \mathrm{Re}^{-1}\nabla^2\zeta, \tag{2.2a}$$

with

$$\zeta = -\nabla^2\psi \tag{2.2b}$$

being the unknown scaled vorticity. Again, polar coordinates such that $(x, y) = r(\cos\theta, \sin\theta)$ are also used later. In the absence of any obstacle $f(x)$ is zero and we suppose then that the uniform shear flow $(\psi, u, v, \zeta, p) = (\frac{1}{2}y^2, y, 0, -1, 0)$ holds everywhere for positive y. With $f(x)$ present, on the other hand, computations are required in general because of the nonlinearity associated with blunt shaped obstacles, in contrast with the previous linear analyses mentioned in the introduction for non-blunt shapes. Computations are considered in Section 3, followed by theory for large Re values in Section 4.

3. Computational methods

Two separate computational approaches were used on (2.1a–e) and/or (2.2a,b) as described below. They were applied to the blunt non-smooth obstacles formed by a vertical thin flap ($x = 0$ for $0 \leqslant y \leqslant 1$) standing normal to the flat horizontal surface $y = 0$ or by a rectangular block placed on the horizontal surface. It has to be acknowledged immediately that the numerical problem is difficult, due partly to the corners on the obstacles and partly to increasing Re and its accompanying multiple scales, which limits the general accuracy and resolution. For that reason and for the sake of comparison we eventually decided to apply the two distinct computational approaches mentioned. One gave interesting results sooner and this is described first below in some detail, followed by the second.

In one approach the numerical scheme used consists of the alternating-direction implicit (ADI) method and a fourth-order accurate compact difference scheme. For this steady problem the equivalent time coordinate in the differenced Equation (2.2a) for the vorticity is treated as fictitious with each time step considered equivalent to an iteration. In the ADI scheme each time step is split into two halves, resulting in two finite-difference equations each of duration $\delta t/2$ where δt is the time step, used in turn over successive time steps. The first equation is implicit in the x-direction while the second is implicit in the y-direction.

Flows that are dominated by convection as here suffer from numerical instability at high values of the Reynolds number. To suppress such instability upwind differencing in the convection terms could be employed. The artificial dissipation introduced by the upwind difference scheme stabilizes the numerical solution at high values of the Reynolds number. The following quasilinearization is used for the convective terms,

$$\left[gu_x\right]^{n+1} = [g]^n[u_x]^{n+1}. \tag{3.1}$$

The superscript n represents the time step. The spatial derivatives in (3.1) are approximated as

$$\left[gu_x\right]_{i,j} = g_{i,j}\left\{u_{i+2,j} - 2u_{i+1,j} + 9u_{i,j} - 10u_{i-1.j} + 2u_{i-2,j}\right\}/(6\delta x) \tag{3.2a}$$

for $g_{i,j}$ positive, and

$$g_{i,j}\left\{-2u_{i+2,j}+10u_{i+1,j}-9u_{i,j}+2u_{i-1,j}-u_{i-2,j}\right\}/(6\delta x) \tag{3.2b}$$

for $g_{i,j}$ negative. The truncation error of this scheme is given by

$$\frac{1}{4}(\delta x)^3\left[g\frac{\partial^4 u}{\partial x^4}\right]. \tag{3.2c}$$

The upwinding produces a truncation error proportional to the fourth derivative of the vorticity. This numerical dissipation stabilizes computations at high Reynolds numbers and in addition does not significantly affect the physical dissipation. The velocities in the convective terms are calculated using the fourth order accurate Hermitian relations and are given by

$$u_{i,j-1}+4u_{i,j}+u_{i,j+1}=3(\psi_{i,j+1}-\psi_{i,j-1})/\delta y, \tag{3.3a}$$

$$v_{i-1,j}+4v_{i,j}+v_{i+1,j}=-3(\psi_{i+1,j}-\psi_{i-1,j})/\delta x, \tag{3.3b}$$

respectively.

The vorticity boundary condition on the surface is approximated by a second order accurate cubic polynomial approximation and is given by

$$\zeta_{i,0}=-(8\psi_{i,1}-\psi_{i,2})/(2(\delta y)^2). \tag{3.4}$$

The boundary condition on ζ along the obstacle is approximated in a similar manner. It may be noted that no boundary condition could or should be prescribed directly on the vorticity at the outer (top) edge of the flap or on the corners of the square obstacle. Following Dennis and Smith [1], in order to avoid these points, we rotate the axes through an angle $\pi/4$ which leaves the vorticity transport equation (2.2a) unaltered and then we approximate the ζ derivatives as before.

At every fictitious time step the Poisson equation (2.2b) for the stream function is solved by a fourth-order accurate compact difference scheme. This fourth-order method considers as unknowns at each discretized point not only the value of the function $g(i)$ itself but also its first $g'(i)$ and second derivatives $g''(i)$. The system is closed by considering the following relationships between the function and its derivatives at three successive discretization points:

$$g'_{i-1}+4g'_i+g'_{i+1}=3(g_{i+1}-g_{i-1})/h+O(h^4), \tag{3.5a}$$

$$g''_{i-1}+10g''_i+g''_{i+1}=12(g_{i+1}-2g_i+g_{i-1})/h^2+O(h^4), \tag{3.5b}$$

where h represents the spatial step of the discretization. The second-order derivatives $g''(i)$ can be expressed as

$$g''_i=-(g'_{i+1}-g'_{i-1})/(2h)+2(g_{i+1}-2g_i+g_{i-1})/h^2. \tag{3.5c}$$

This expression is fourth-order accurate. In order to reduce the number of unknowns, the second-order derivatives can be eliminated from the governing equations through the relation (3.5c). Besides higher accuracy, another advantage of this method is that it takes into account the boundary conditions on both ψ and its first-order partial derivatives which are data of the physical problem. This method is described in detail by Loc and Bouard [11].

The computational procedure starts by assuming initial values for $\zeta_{i,j}$ and $\psi_{i,j}$ at all mesh points. Using the available values of the stream function, the vorticity transport equation is solved for $\zeta_{i,j}$. Then utilizing the values of $\zeta_{i,j}$, the Poisson equation for the stream function is solved to update $\psi_{i,j}$. At the end of each time step new estimates of $\zeta_{i,j}$ and $\psi_{i,j}$ are obtained by this process. The procedure is repeated as the computational scheme progresses in time until a certain relative error criterion, preselected as a condition for convergence, is satisfied.

As rapid changes in the flow take place around the obstacle, we included more densely packed grid points around the obstacle. Further away from the obstacle grid stretching is applied, defined by

$$x_{i+1} = x_i + \beta(x_i - x_{i-1}), \tag{3.6}$$

where $\beta = \frac{5}{4}$. Similar operations are made for $y(j)$. To check on how much the numerical solution is dependent on the grid size, the grid sizes around the obstacle were made to range between $0{\cdot}001 \times 0{\cdot}001$ and $0{\cdot}01 \times 0{\cdot}01$ at selected Reynolds numbers. The effects of grid sizes on the solution are found to be minimal (see later figure). We found that a grid size $0{\cdot}005 \times 0{\cdot}005$ near the obstacle produces the optimal solution. The fictitious time step was taken as $0{\cdot}001$ originally but was then increased at subsequent times t.

It may be noted that the fourth order accurate compact difference scheme cannot be used where variable grid sizes are considered. Away from the obstacle, where variable grid sizes are used, the Poisson equation for stream function is solved through a central difference scheme along with the successive over relaxation technique.

A second computational approach has also been used on the flow problem. Only preliminary results from this were available at the time of writing and we hope to report fully on this separate approach in the near future. For now we note that this approach is based on Dennis and Hudson's [12], it is a fourth order scheme and it proves to be both accurate and stable: see the comparisons in [12] itself. While the results from the second approach are still to be regarded as tentative so far, and are for the vertical thin flap only, subsequent comparisons in Section 5 with results from the first approach above are found to be affirmative.

Results are described in Section 5.

4. Theory

The theory presented in this section concerns the flow properties at large Re specifically, although without doubt small Re is also of interest. It is predicted, and later found, that for large Re values, and for *any* blunt obstacle, the length of upstream influence is markedly large, as is the upstream separation distance, and the downstream influence length and reattachment distance are even larger.

The obstacle shape is taken as suitably smooth for now. Non-smooth shapes are addressed at the end of this section. Some guidance for the theory comes from Smith [13], Smith and Walton [5], suggesting a beginning on $O(1)$ scaled streamwise lengths.

First, on the actual obstacle $f(x)$ a thin attached boundary layer is produced, with pressure variations of order unity, followed downstream by a thin separated free shear layer. The latter adjusts its position ($F(x)$ say) to make the pressure variation almost negligible inside the accompanying long eddy of recirculating fluid, broadly, over length scales x of order one, and in consequence the height $F(x)$ of the free shear layer tends to a (positive) constant further downstream, so that $F(\infty) > 0$. The corresponding pressure and the stream-function perturbation both tend to $-\frac{1}{2}F^2(\infty)$.

Second, in the outer majority of the flow inviscid forces dominate. So, sufficiently far away, on a long x scale where the disturbance to the surrounding uniform-shear motion is relatively small, $u - y$ and v satisfy Laplace's equation (whereas p satisfies $y\nabla^2 p = 2\partial p/\partial y$). The equation is subject to farfield decay which is to be found and to matching the disturbance of the stream function, $\psi - \frac{1}{2}y^2$, with $-\frac{1}{2}F^2(\infty)$ as y decreases towards zero in the downstream portion of the flow and with zero in the upstream portion. Hence the fundamental decay is algebraic, being given simply by

$$u - y \sim \Gamma r^{-1} \cos\theta, \tag{4.1}$$

for large distances r, with the constant $\Gamma \equiv F^2(\infty)/(2\pi)$ and with the corresponding stream-function disturbance being $\Gamma(\theta - \pi)$. The above result coincides in fact with the source-like effect of the obstacle shape combined with the free-shear-layer shape/positioning, which yields an overall jump in the mass flux over a long streamwise scale, coupled with the Bernoulli relation for the pressure. In particular, the slip induced from (4.1) near the flat surface decays as the inverse of distance.

Third, close to the flat surface in the upstream portion of the flow a viscous wall layer must be provoked. There the velocity u is $y + 0(|x|^{-1})$, from (4.1), but the viscous y scale has to be of order $\mathrm{Re}^{-1/3}\,|x|^{1/3}$ of course in a uniform shear motion, from the inertial-viscous balance of $y\partial/\partial x$ against $\mathrm{Re}^{-1}\partial^2/\partial y^2$. Therefore we equate $\mathrm{Re}^{-1/3}\,|x|^{1/3}$ with $|x|^{-1}$, in terms of orders of magnitude, implying the long streamwise length scale $|x| \sim \mathrm{Re}^{1/4}$ for the viscous-inviscid interaction that is necessary for nonlinear upstream influence and in particular the possibility of separation upstream. It follows that in the viscous wall layer the velocity components and pressure are $\mathrm{Re}^{-1/4}U$, $\mathrm{Re}^{-3/4}V$, $\mathrm{Re}^{-1/2}P$ to leading order, with x, y scaled as $\mathrm{Re}^{1/4}X$, $\mathrm{Re}^{-1/4}Y$ in turn, and the controlling equations from (2.1a–c) become the interactive boundary-layer system

$$\frac{\partial U}{\partial X} + \frac{\partial V}{\partial Y} = 0, \qquad U\frac{\partial U}{\partial X} + V\frac{\partial U}{\partial Y} = -P'(X) + \frac{\partial^2 U}{\partial Y^2}, \tag{4.2a,b}$$

for the order-one quantities $U(X, Y)$, $V(X, Y)$, $P(X)$. There is negligible normal pressure gradient because of (2.1c). The boundary conditions require no slip along $Y = 0$ for all negative X values and

$$U \sim Y + \Gamma X^{-1} \text{ as} Y \to \infty, \tag{4.2c}$$

in view of (4.1) holding in the motion outside. Here the constant Γ is defined just after (4.1) and is positive but the imposed displacement in (4.2c) is upward, *i.e.* $U - Y$ is negative, as X is negative, thus indicating an increasing tendency towards flow separation as X increases. The solution of the reduced problem (4.2a–c) starts as a small perturbation from the incident profile $U = Y$ far upstream at large negative X and thereafter can be obtained from a single forward march in X, at least up to separation (flow reversal). Fortunately this reduced problem can be normalized to one solved numerically by Smith and Walton [5], even though the present work is a generalization of theirs to allow for the finite ratio of the length of the obstacle to its width in the present configurations and for the variable eddy height $F(\infty)$ downstream, as well as being a simplification in respect of the source effect (4.1). Separation is found to occur at $X = -0{\cdot}142\,F(\infty)^{3/2}$. Beyond this station a FLARE (after Flügge-Lotz and Reyhner) approximation in which the first term in (4.2b) is neglected wherever U is negative seems to work fairly well as usual numerically, permitting continued forward marching. The

flow solution continues towards $X = 0-$, that is, towards order-one length scales around the obstacle, developing there an asymptotic grossly separated form in line with the displacement effect in (4.2c). Thus whereas the outer inviscid response exhibits quite simple decay lasting over great distances, in (4.1), the near-surface viscous response is rather more intricate, its perhaps most significant feature being the predicted behaviour

$$x_1 = -0.142(F(\infty))^{3/2}\mathrm{Re}^{1/4} \tag{4.3}$$

of the upstream separation point at large Reynolds numbers.

Fourth, after the increasingly separated motion beyond the station (4.3) joins to the thinner boundary layer on the obstacle itself, as described previously, this thin boundary layer proceeds downstream through a second smooth separation, on/from the obstacle, to form the thin free shear layer also mentioned previously. In particular if the height of the real obstacle is negligible downstream so that $f(\infty)$ is zero then that of the effective obstacle, $F(\infty)$, is nonzero as the free shear layer emerges almost horizontally atop the long eddy far downstream on the above length scales. Closure of that downstream eddy and a flow-reattachment process to the surface then take place on the much longer length scale where x is of order Re, with the characteristic y scale being of order unity. Accordingly the boundary-layer equations (as in (4.2a,b)) again describe the process there, given that u, v, p are expected to scale with the orders $1,\ \mathrm{Re}^{-1},\ 1$ in turn, owing to the boundary conditions in (2.1e) (applied as in [14]) and the outer decay in (4.1). The starting profile, however, for the downstream reattachment process is discontinuous, at $y = F(\infty)$, or has discontinuous derivatives, in order to merge with the incident separated-motion properties further upstream. The flow solution in normalized form can be deduced from Smith and Daniels [14], fortunately, and in particular it gives the prediction

$$x_2 = 0{\cdot}076(F(\infty))^3\mathrm{Re} \tag{4.4}$$

for the downstream reattachment point at large Reynolds numbers. This, while subject to certain assumptions about the starting profile noted above, actually confirms the earlier arguments leading to (4.1)–(4.3) on the shorter length scales.

The above points are the major points, and more analytical detail is as in [5],[13] essentially, but the most relevant brief comments here are the following. The argument supposes that the effective height parameter $F(\infty)$ is typically of order unity, whether due to the actual obstacle height $f(\infty)$ being nonzero or to the long eddy shape downstream. So the reasoning extends to non-smooth obstacles also, such as a normal (vertical) thin flap or a rectangular block as in the numerical cases of Sections 3,5, although the theoretical separation from the obstacle is different then and indeed may be multiple. The scales, by the way, in (4.3),(4.4), are such that if Re, x, y are based on the eddy height instead of obstacle height then the factors $F(\infty)$ are replaced by unity. Further, the quite long, algebraic, upstream-influence scale exemplified by (4.3) contrasts with those in Smith [13], Dennis and Smith [1] which are only logarithmic, the distinction stemming from the slow algebraic decay to the state of uniform shear as in (4.1). Finally here, similar reasoning may well apply also in three-dimensional motions under uniform near-surface shear at large Re values.

5. Results and comparisons

The flow past a variety of obstacle shapes has been studied numerically by means of the methodology described in Section 3. The results shown here are all either for a vertical thin

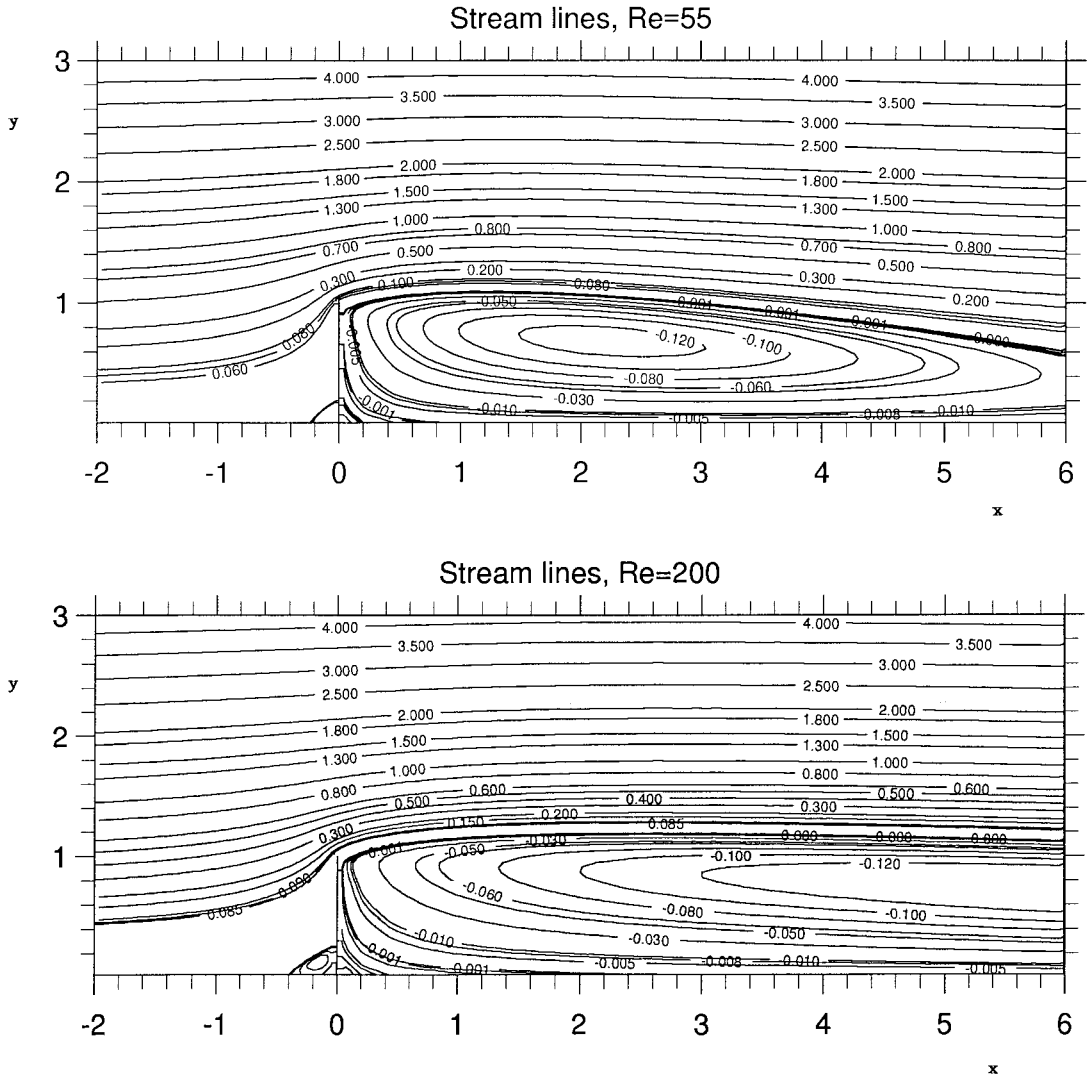

Figure 2. Computational results for the flow streamlines at Re $= 55, 200$, for (a,b) the vertical-flap shape and (c,d) the square-block shape.

flap of nondimensional height 1 $(= f(0))$ or for a square block of nondimensional height 1, mounted on the horizontal surface.

The main computational results are presented in Figures 2–6, showing the induced pressure gradients, surface shears, streamlines and other properties. Thus Figure 2 gives the streamline plots determined at the particular representative values 55 and 200 of the Reynolds number Re, for the vertical flap and the square block, while Figure 3 gives vorticity curves and velocity vectors, again for two Re values. In Figure 3(a) the main contour values of the vorticity are marked except for the most negative values which are -12, -8, -7, -6, -5, and similarly the most negative vorticity values shown in Figure 3(c) are -10, -5. Figure 4 then shows the pressure gradients produced along the horizontal surface $y = 0$ at Re equal to 100, and Figure 5 presents the computed results at Re of 100 for the horizontal surface vorticity,

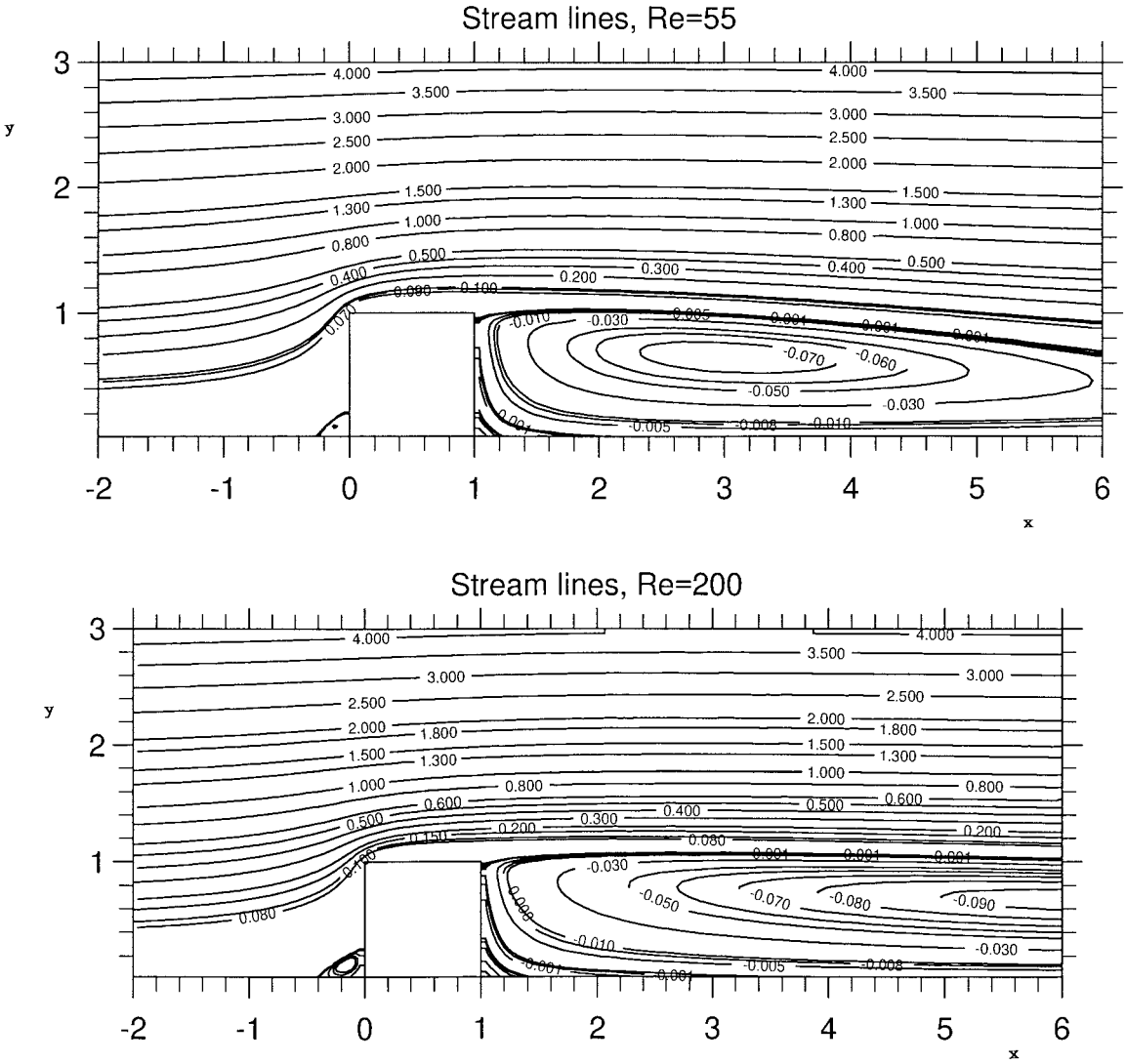

Figure 2. Continued.

including a study of grid-size effects which suggests that the results are of quite high accuracy up to that Reynolds number.

Figure 6(a,b) provides plots of the upstream separation and downstream reattachment positions x_1, x_2, versus Re, which are reasonably sensitive measures of the upstream and downstream eddy features. The results shown are as deduced from the direct computations of the surface vorticity and from the theory summarized by (4.3), (4.4), for both the vertical-flap case and the square-block case. Any slight "wiggles" in the computational results in Figure 6 are due to the interpolation used to estimate the values of x_1, x_2 numerically; while in the theory the quantity $F(\infty)$ is taken mostly as the obstacle height. We should add that most of the results shown are from the first computational method described in detail in section 3, but comparisons between results from both computational approaches used are also presented in Figures 5(a), 6(a), 6(b) for the case of the flap. Given the clear extrapolation effects in Figure 5(a), and the fact that only the results obtained from the smallest grid used so far in

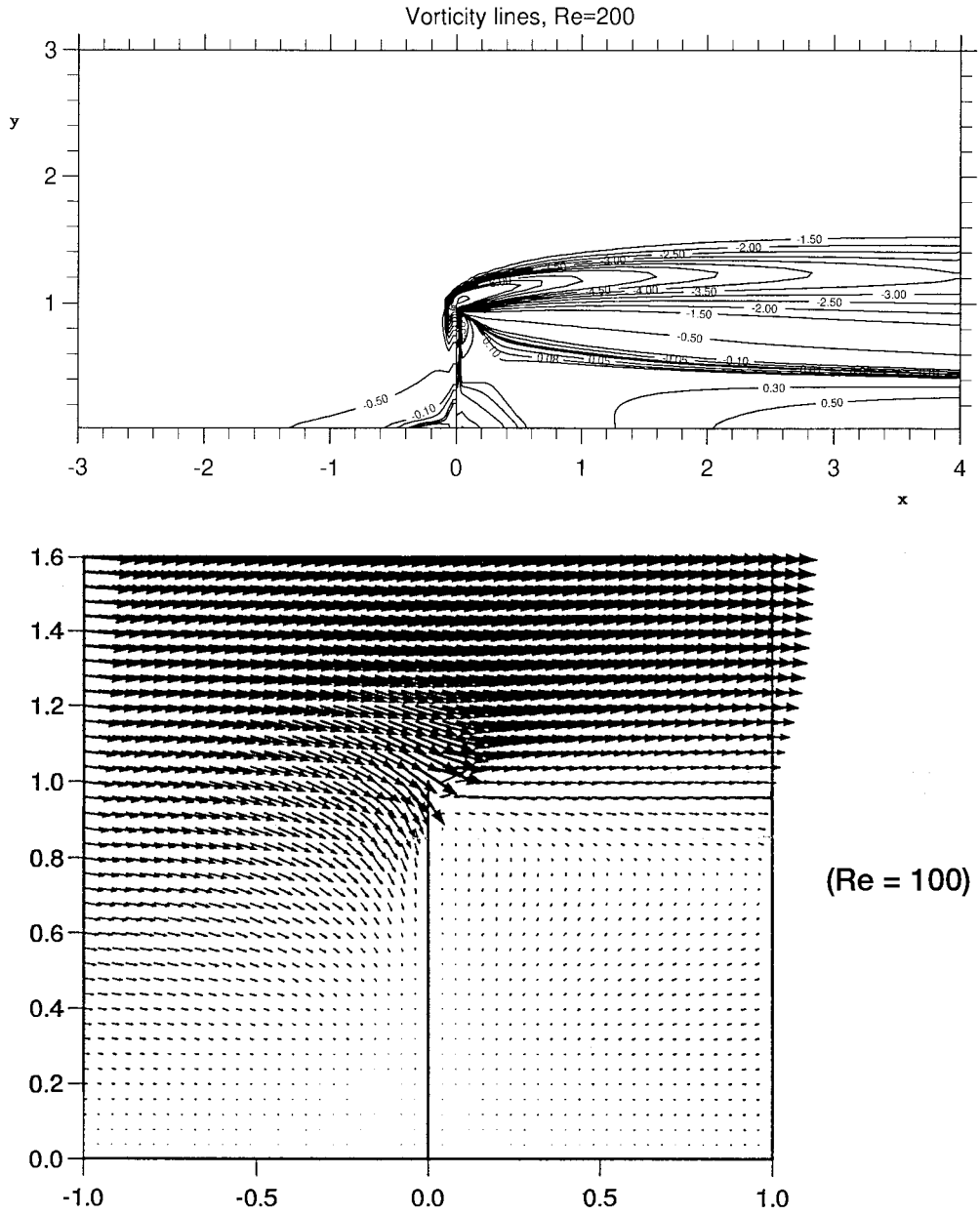

Figure 3. Computed vorticity contours and velocity vectors, at various Re, for (a,b) vertical flap at Re = 200, 100 respectively and (c,d) square block at Re = 200.

the second computational method are plotted in Figures 6(a), 6(b), the sets of results would appear to be consistent and accurate.

The above comparison between the computations and the theory in the determination of x_1, x_2 in Figure 6(a,b) indicates that there is fairly good quantitative agreement on the separation and reattachment positions, from lowish Re values, despite there being only one term, the leading term, in (4.3), (4.4). Earlier comparisons on separation and reattachment points for other shapes addressed experimentally by Klebanoff and Tidstrom [15] and numerically

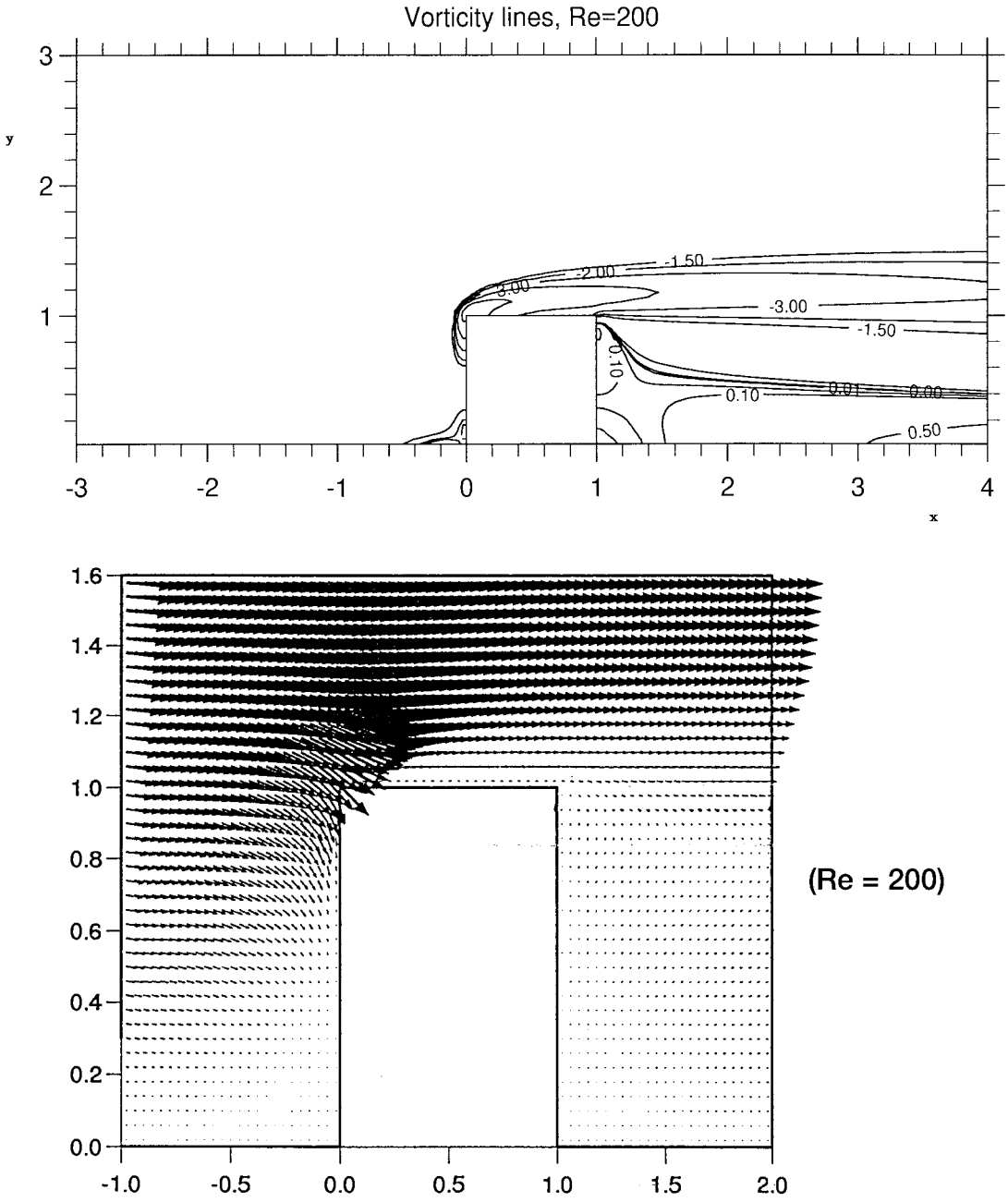

Figure 3. Continued.

by Bogolepov [16] are noted by Smith and Walton [5], Smith [7]. Even more recent computational results by Ngo Boum *et al.* [17] also agree at least qualitatively with the present ones as regards the trend of the downstream reattachment position x_2 with increasing Re, although this last paper puts forward an (unjustified) formula different from the present (justified) one (4.4) and it also overlooks the smaller separation arising upstream, possibly due to lack of numerical resolution.

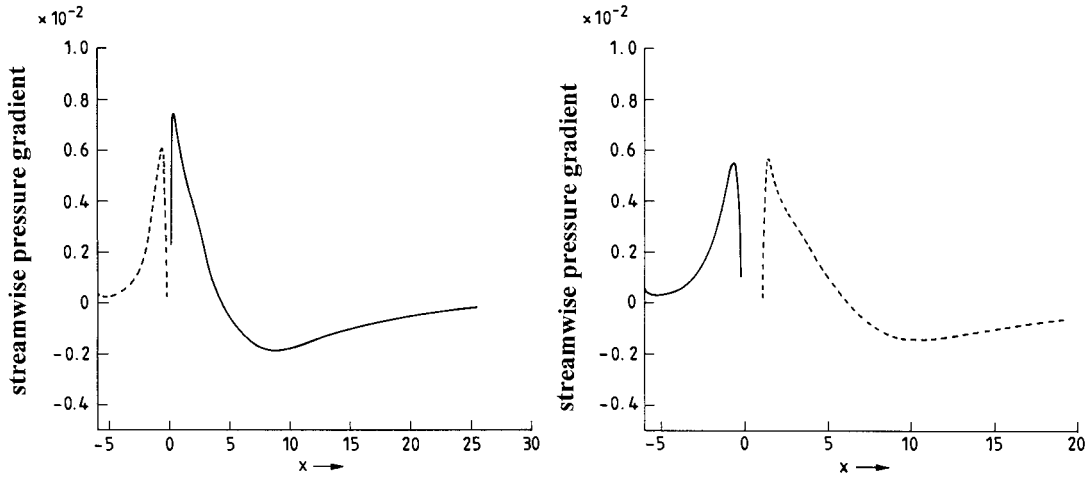

Figure 4. Computed pressure gradients $\partial p/\partial x$ on the horizontal surface $y = 0$ at Re $= 100$; (a) flap, (b) block.

Returning to the present computations, we note that another point of comparison concerns the position of maximum surface pressure gradient upstream. The theory according to Figure 4 of [5] predicts the above position to be approximately twice as far upstream as the separation position x_1, and the computational results in our Figures 4,5 are reasonably in line with this at the shown Re values. The whole trend of the surface pressure gradient inferred from Figure 4 of [5] is also in line with, although somewhat higher than, the results at Re of 100 in our Figure 4(a,b). There is in addition good qualitative agreement, between the present computations and the present theory, on the overall flow structure, in particular the presence of attached or detached thin layers as Re increases. Indeed, an increase in the value of $F(\infty)$ suggested perhaps by the streamline plots of Figure 2 would bring the theoretical and computational values even closer together; see Figure 6(b). Moreover the behaviour of the upstream separation point x_1 is clearly in response to the pressure feedback influence from the presence of the blunt obstacle, which leads in virtually all cases to a streamwise rise in the horizontal surface pressure ahead of the obstacle, that is, a slight adverse pressure gradient there. Hence on inviscid reasoning the slight, induced, effective slip velocity u_w then falls in the streamwise direction but this effect is on top of the original incident linear velocity profile of (2.1e) and so acts near the wall as an increasing *displacement* response [that is, of the form $y + u_w(x)$ with $u_w(x)$ monotonically decreasing with x]. It is this last response that provokes the upstream separation and hence specifically the result (4.3). Again theory and computation appear to be in agreement on the main physics of the separating flow structure here.

6. Further comments

The flow past a blunt obstacle mounted on an otherwise flat surface is intricate as well as fascinating even in the steady laminar two-dimensional regime. Its accurate determination seems to be aided considerably by the combination of theory and direct computing, the former emphasizing the reduced equations of motion that capture the major physics at large Reynolds numbers whereas the latter address the full equations at reduced Reynolds numbers. The fairly close agreement between the results of the two as investigated in the previous section would

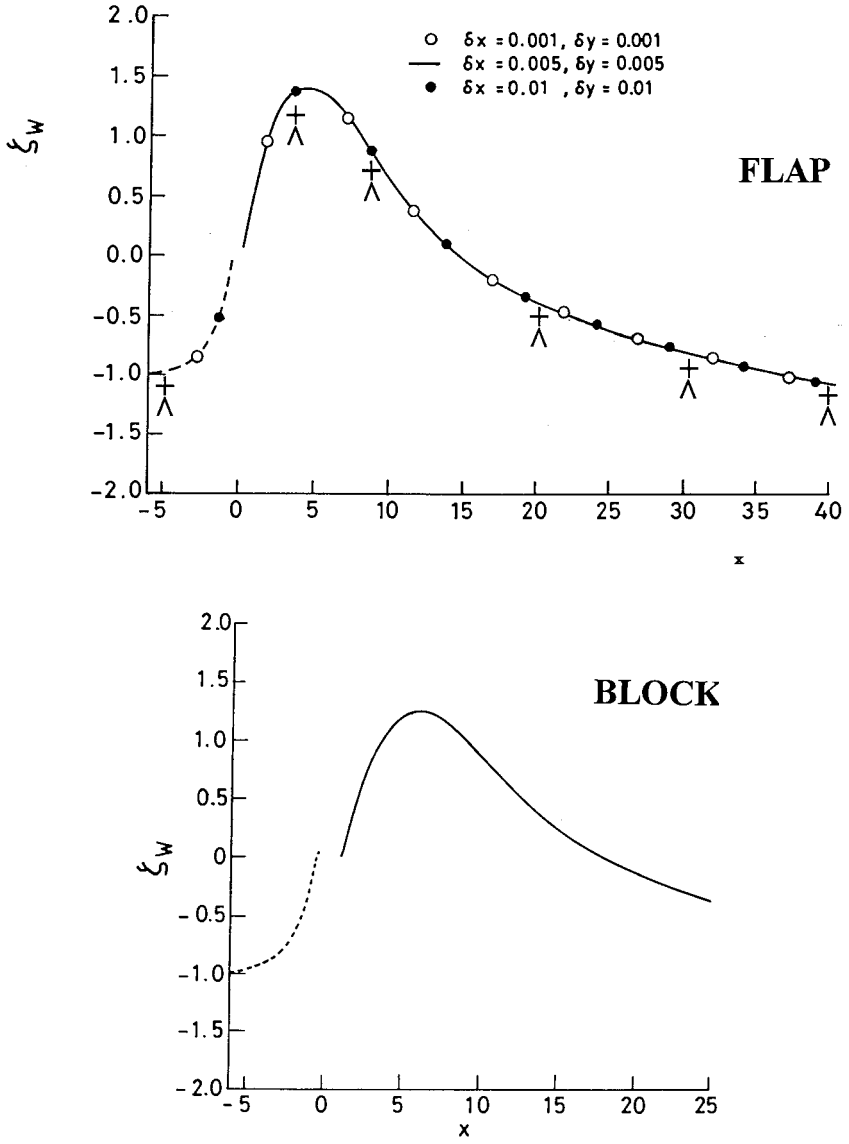

Figure 5. Computational results for the horizontal surface shear ζ at $y = 0$ (for Re $= 100$), and a study on the influences of the grid sizes. (a) Flap. (b) Block. Results from the separate computational method are also shown in (a), for grid spacings 0·05, 0·01 ($\wedge$, $+$, respectively).

appear to enhance the value of both. This is especially so in view of the moderate values of Reynolds number involved in all the comparisons.

Extensions of the work would be interesting on both the direct computational and the theoretical sides. An extension to higher blunt obstacles could allow for the effects of interference from the full velocity profile, acting across the boundary layer, internal flow or other more global motion. Interesting experimental investigations have been made by Giguère, Dumas and Lemay [6] on the Gurney flap and its scaling concerning lift-to-drag ratio of an airfoil. This flap is typically a tiny fence standing normal to the airfoil surface, near the trailing edge, as in their Figure 1. For a particular airfoil they note that Liebeck earlier found increased lift

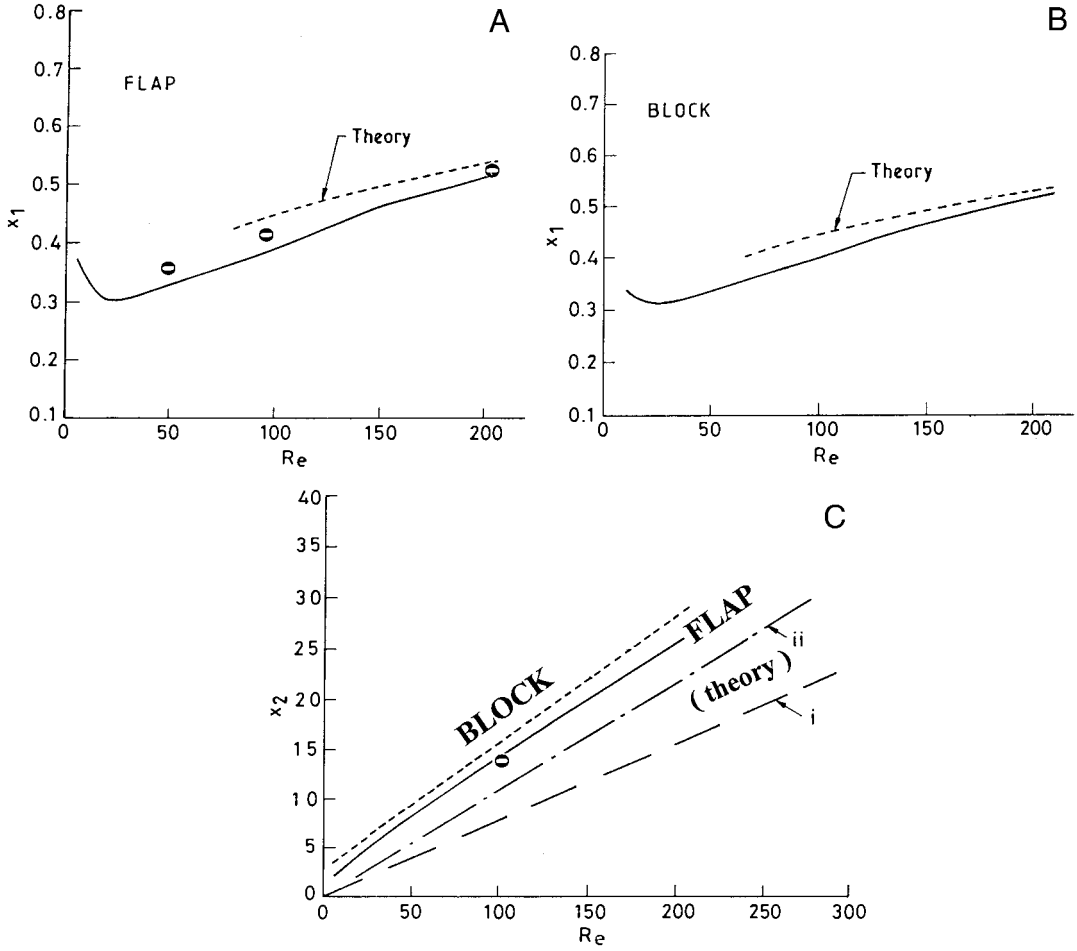

Figure 6. Comparisons, for the vertical flap and the square block. (a, b) Theory and computations for the upstream separation and downstream reattachment positions x_1, x_2 versus Re. (Results from the separate computational method are included as open circles for the flap case, for the smallest grid used.) In (b) curve (i) is from (4.4) with $F(\infty)$ taken as the obstacle height $f(\infty)$, while (ii) has $F(\infty)$ taken as $1{\cdot}115\,f(\infty)$.

and reduced drag for high lift coefficients from the addition of a flap of height 1.25% chord, and the benefits of the device were maximized with heights between 1% and 2%. Results in broadly the same vein are given in their Figures 1,2. Although they give the opinion that the physical mechanism associated with this device is still an open question, the present view is that it is the pressure-feedback mechanism of Section 4 extended to higher obstacles exactly as above. Another extension, to unsteady motions, seems desirable in the context of arterial blood flows for example and likewise concerning the possibility of flow transition. Extending the work to three-dimensional flows can also be done in principle, some theoretical studies by Professor S.N. Brown, Mr. N.C. Ovenden and F.T.S. being in progress.

References

1. S.C.R. Dennis and F.T. Smith, Steady flow though a channel with a symmetrical constriction in the form of a step. *Proc. R. Soc. London* A 372 (1980) 393–414.

2. R.W. Mei and A. Plotkin, Navier Stokes solutions for laminar incompressible flows in forward-facing step geometries. *A.I.A.A. J.* 24 (1986) 1106–1111.
3. F. Durst and T. Loy, Investigations of laminar flow in a pipe with sudden contractions of cross sectional area. *Comp. Fluids* 13 (1985) 15–36.
4. D.J. Savin, F.T. Smith and T. Allen, Transition of free disturbances in inflectional flow over an isolated roughness. *Proc. R. Soc. London* A 455 (1999) 491–541.
5. F.T. Smith and A.G. Walton, Flow past a two- or three-dimensional steep-edged roughness. *Proc. R. Soc. London* A 454 (1998) 31–69.
6. P. Giguère, G. Dumes and J. Lemay, Gurney-flap scaling for optimum lift-to-drag ratio. *A.I.A.A. J.* 35 (1997) 1888–1890.
7. F.T. Smith, On physical mechanisms in two- and three-dimensional separations. Theme Issue, *Phil. Trans. R. Soc. London* A (2000) in press.
8. R.W. Johnson (ed.), *The Handbook of Fluid Dynamics.* Boston; CRC Press, Boston (1998).
9. K. Stewartson, On the flow near the trailing edge of a flat plate, II. *Mathematika* 16 (1969) 106–121.
10. F.T. Smith, Laminar flow over a small hump on a flat plate. *J. Fluid Mech.* 57 (1973) 803–824.
11. T.P. Loc and R. Bouard, Numerical solution of the early stage of the unsteady viscous flow around a cylinder: a comparison with experimental visualisation and measurements. *J. Fluid Mech.* 160 (1985) 93–177.
12. S.C.R. Dennis and J.D. Hudson, Compact h^4 finite-difference approximations to operators of Navier-Stokes type. *J. Comp. Phys.* 85 (1989) 390–416.
13. F.T. Smith, The separating flow through a severely constricted symmetric tube. *J. Fluid Mech.* 90 (1979) 725–754.
14. F.T. Smith and P.G. Daniels, Removal of Goldstein's singularity at separation in flow past obstacles in wall layers. *J. Fluid Mech.* 110 (1981) 1–37.
15. P.S. Klebanoff and K.D. Tidstrom, Mechanism by which a two-dimensional roughness element induces boundary layer transition. *Phys. Fluids* 15 (1972) 1173–1188.
16. V.V. Bogolepov, Separated flows near an upward-facing step. Presentation at Euromech Colloquium, Manchester, July 6–9, 1998, and private communication.
17. G.B. Ngo Boum, S. Martemianov and A. Alemany, Computational study of laminar flow and mass transfer around a surface-mounted obstacle. *Int. J. Heat Mass Transfer* 42 (1999) 2849–2861.